JOURNAL OF PROPULSION AND POWER
Vol. 26, No. 4, July–August 2010

Influence of Intake Orientation on Ramjet Performance

Dirk Herrmann* and Ali Gülhan†
DLR, German Aerospace Center, 51147 Cologne, Germany

DOI: 10.2514/1.47140

The dependency of the performance of a two-dimensional intake for air-breathing missiles on intake orientation has been investigated experimentally. The main objective of the study is to identify the ideal intake position on the missile body. Experiments have therefore been carried out at combinations of different angles of attack and different roll angles of the intake and the missile body. All tests were performed at the intake design Mach number of 2.5 and at angles of attack ranging from 0 to 30° in the Trisonic Wind Tunnel Cologne. The results show that the ideal intake position depends on boundary-layer flow, flow separation, and vortices, which vary with different angles of attack. Furthermore, some intake orientations show a mass flow rise on the windward side, where the intake could be located.

Nomenclature

A	=	cross-sectional area, m^2
a	=	speed of sound, $m\,s^{-1}$
c_P	=	pressure coefficient, $(p - p_0) \cdot q_0^{-1}$
D	=	diameter of the missile, m
L	=	length of the missile, m
l	=	reference length, m
M	=	Mach number, $v \cdot a^{-1}$
$\dot{m}$	=	mass flow rate, $kg\,s^{-1}$
p	=	pressure, $N\,m^{-2}$
p_{pitot}	=	Pitot pressure, $N\,m^{-2}$
q	=	dynamic pressure, $N\,m^{-2}$
R	=	specific gas constant for air, 287.15 $J\,kg^{-1}\,K^{-1}$
Re	=	Reynolds number, $\rho \cdot v \cdot l \cdot \mu^{-1}$
T	=	temperature, K
v	=	flow velocity, $m\,s^{-1}$
x, y, z	=	Cartesian coordinates, m
α	=	angle of attack
Δ	=	difference
κ	=	heat capacity ratio
μ	=	viscosity, $kg\,m^{-1}\,s^{-2}$
ρ	=	density, $kg\,m^{-3}$
ϕ	=	angle of roll

Subscripts

0	=	freestream condition
3	=	position of measurement pipe cross section where pressure measurements are performed
4	=	position of throttle's critical cross section
design	=	design (shock-on-lip)
intake	=	position of intake relative to main missile body
lip	=	position at cowl lip
missile	=	position on main missile body
st	=	static condition
t	=	total condition
throat	=	position at throat

Received 11 September 2009; revision received 12 March 2010; accepted for publication 14 April 2010.

*Research Scientist, Supersonic and Hypersonic Technology Department of the Institute of Aerodynamic and Flow Technology, Linder Höhe; dirk.herrmann@dlr.de.

†Head of Department, Supersonic and Hypersonic Technology Department of the Institute of Aerodynamic and Flow Technology, Linder Höhe; ali.guelhan@dlr.de. Member AIAA.

I. Introduction

SUPERSONIC missiles with air-breathing propulsion use the oxygen for combustion from the atmosphere, contrary to rocket-motor-driven missiles, which carry the oxygen for combustion with them. A ramjet has no rotating parts and needs to reach a certain speed and altitude for operation. To keep combustion stable, the intake must provide the engine with a sufficient air mass flow and the required pressure recovery in all flight conditions. It is therefore important to identify the ideal intake position on the missile for good ramjet engine performance even at high angles of attack [1,2].

Several studies have been carried out on optimizing intake performance using internal intake components. Amongst other parameters, intake performance also depends on upstream flow. Different research groups have investigated the effect of major component properties on intake performance, e.g., the modification of the intake's internal geometry [3] and side walls [4]. Variations of chin-intake entrances reveal different effects on performance [5] and studies at the position of the intake's diffuser were carried out to avoid flow separation [6]. Other studies included unstart criteria and intake buzzing [7], which must be prevented [8] to ensure the functionality of the ramjet and prevent destruction of the engine structure. One technique is to control the intake's normal shock by adjusting internal parts of the intake [9,10]. All examples deal with intake design and a given unchangeable main missile design. On the basis of still open issues from these studies, the influence of the upstream flow on intake performance was identified as one of the key issues.

Therefore, the main purpose of this study is to clarify the influence of the main flow parameters on intake behavior in terms of the intake's position on the missile body. This paper describes the experimental techniques used for the experiments and results with respect to the effects of intake position on performance at a freestream Mach number of $M_0 = 2.5$ with angles of attack ranging from $0° \leq \alpha \leq 30°$. Shown among other things are the specific effects of windward and leeward flow at small and large angles of attack, and the comparison of possible intake positions.

In Sec. II, the wind tunnel and intake models are described. Experiments with varying intake positions along the missile body with different roll angles of the intake and missile body are described in Sec. III. Furthermore, the intake characteristics, i.e., pressure recovery and mass flow rate, are analyzed with schlieren images, oil flow visualization and pressure measurements. Finally, the main results of this study are summarized, and some conclusions are given.

II. Experimental Setup

A. Trisonic Wind Tunnel Cologne

The experiments were conducted in the Trisonic Wind Tunnel (TMK) [11] of the German Aerospace Center (DLR) in Cologne. The TMK is a blow-down wind tunnel with a cross section of

0.6 m × 0.6 m. It is equipped with a flexible nozzle, which can be adjusted while testing. A test duration of 60 s is possible, depending on the Mach and Reynolds number. Its standard Mach number range is $1.25 < M_0 < 4.5$. Mach numbers up to 5.7 can be achieved with the aid of a storage heater and an ejector. The ejector facilitates a Reynolds number variation by a factor of up to seven. For Mach numbers of $0.5 < M_0 < 1.2$, a transonic test section with perforated walls is available.

B. Model and Flow Conditions

The basic intake model (without boundary-layer bleed) with mixed compression was presented and analyzed in [6] with other setups. This three-ramp intake is designed for a freestream Mach number of $M_{\text{design}} = 2.5$ (shock-on-lip) and the intake's compression ratio is 5.2%. Using Eq. (1) in accordance with [12], the compression limit for self-starting is calculated with the entrance plane A_{lip} at the cowl lip, its Mach number M_{lip} and the throat's plane A_{throat}

$$\frac{A_{\text{lip}}}{A_{\text{throat}}} = \frac{1}{M_{\text{lip}}} \cdot \left[\frac{(\kappa+1)\cdot M_{\text{lip}}^2}{(\kappa-1)\cdot M_{\text{lip}}^2+2}\right]^{\frac{\kappa}{\kappa-1}} \cdot \left[\frac{\kappa+1}{2\cdot\kappa\cdot M_{\text{lip}}^2-(\kappa-1)}\right]^{\frac{1}{\kappa-1}} \cdot \left[\frac{2+(\kappa-1)\cdot M_{\text{lip}}^2}{\kappa+1}\right]^{\frac{\kappa+1}{2\cdot(\kappa-1)}} \tag{1}$$

The compression limit [12,13] at $M_0 = 2.5$ is 13.9% and 7% at $M_0 = 2.1$. The intake should self-start at a Mach number below 2.1, because the intake's compression ratio is still smaller.

The intake is mounted on the wind tunnel support. The intake roll position can be freely varied around its axis. Downstream, the main missile body is attached to the wind tunnel support behind the intake, so that the axis of roll is the same as the intake's. A spline shaft assembly is used for this attachment to withstand the aerodynamic loads up to an angle of attack of $\alpha = 30°$. It is possible to roll the missile body around the rolling axis in 7.5° steps. The roll position of the intake around its own axis, i.e., the orientation of the ramps with respect to the missile, and the roll position of the intake with respect to the missile body, i.e., the circumferential position at the intake, can therefore be varied independently. The missile body consists of a 26° cone and a cylindrical body (diameter $D = 70$ mm) of variable length. Next to the main cylindrical element with a length of $L/D = 5$, there are two cylindrical elements with the length of $L/D = 2$. Therefore, three different axial intake positions $L/D = 5$, $L/D = 7$ and $L/D = 9$ can be adjusted. The assembled model mounted in the TMK can be seen in Fig. 1.

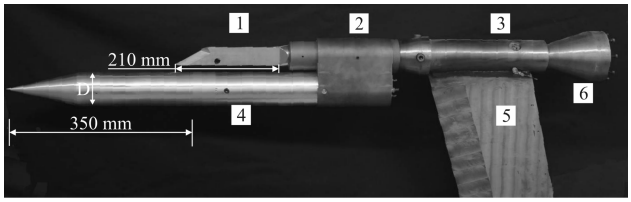

1 Intake 2 Spline shaft assembly 3 Measurement pipe
4 Missile body (L/D = 5) 5 Model support 6 Throttle

Fig. 1 Assembled intake model at $\alpha = 0°$.

The model was tested between angles of attack of $0° \le \alpha \le 30°$ at increments of 3°, between the intake roll angles of $0° \le \phi_{\text{intake}} \le 270°$ (in relation to the missile's surface) at increments of 90° and (by exploiting the symmetry) between the missile body roll angles of $0° \le \phi_{\text{missile}} \le 180°$ at increments of 15°. To gain a better understanding of the different roll angles, Fig. 2a shows a sketch of the front view of the assembled model seen in Fig. 1. Figure 2 illustrates a roll angle variation of the intake, wherein the intake is rolled from $\phi_{\text{intake}} = 0°$ (Fig. 2a) to $\phi_{\text{intake}} = 270°$ (Fig. 2d) at a missile roll angle of $\phi_{\text{missile}} = 0°$. The responding photos are shown below. The roll angle variation of the missile is shown in Fig. 3 (with photos below), where the missile roll angle is changed from $\phi_{\text{missile}} = 0°$ to $\phi_{\text{missile}} = 180°$, while the intake roll angle relating to the missile's surface stays constant at $\phi_{\text{missile}} = 90°$. All angles have an inaccuracy of ±0.1°, defined by the digital protractor. These test conditions are given in Table 1 and the flow condition is given in Table 2 including the unit Reynolds number

$$Re = \frac{\rho_0 \cdot v_0 \cdot l}{\mu_0} \tag{2}$$

with the reference length of 1 m. The accuracy of measurement values is given in Table 3 as percentage error of the expected measurement range. Theses values based on manufacturer's instruction and [11], where Pitot measurements are performed amongst other things.

C. Measurement Technique

To investigate intake performance at different positions on the missile's body, mass flow and pressure recovery have to be measured and illustrated. The measurement configuration for this purpose is shown in Fig. 4.

The measurement configuration consists of the intake, which is mounted on the front of the measurement pipe, and the throttle, which is connected to the downstream end. The throttle was calibrated using a calibration standard based on orifice technology [14,15], where the pressure is measured differential through the orifice plate. The mass flow rate through the throttle is determined with the sonic flow method, where the flow chokes and a sonic line is induced in the throttle. Another function of the throttle is to simulate the pressure in the combustion chamber. This pressure is varied by

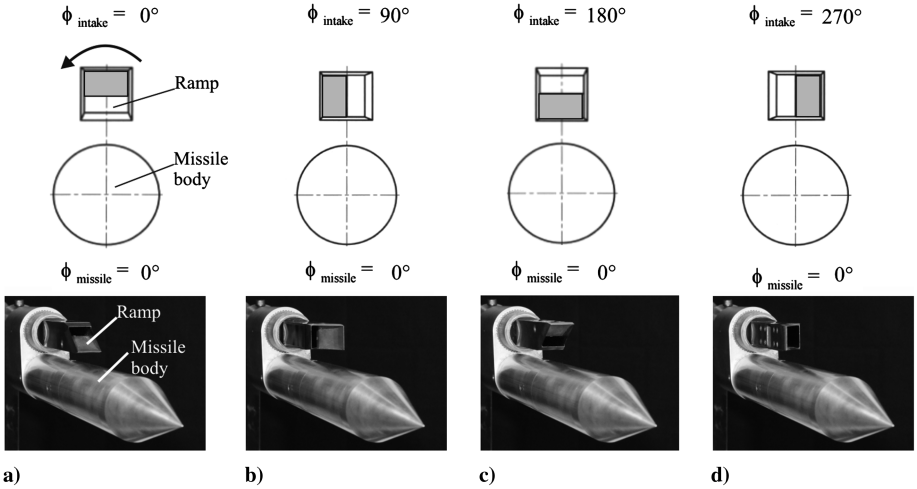

Fig. 2 Sketch of front view and photo of model at an roll angle of the missile of $\phi_{\text{missile}} = 0°$ and roll angles of the intake of a) $\phi_{\text{intake}} = 0°$, b) $\phi_{\text{intake}} = 90°$, c) $\phi_{\text{intake}} = 180°$, and d) $\phi_{\text{intake}} = 270°$.

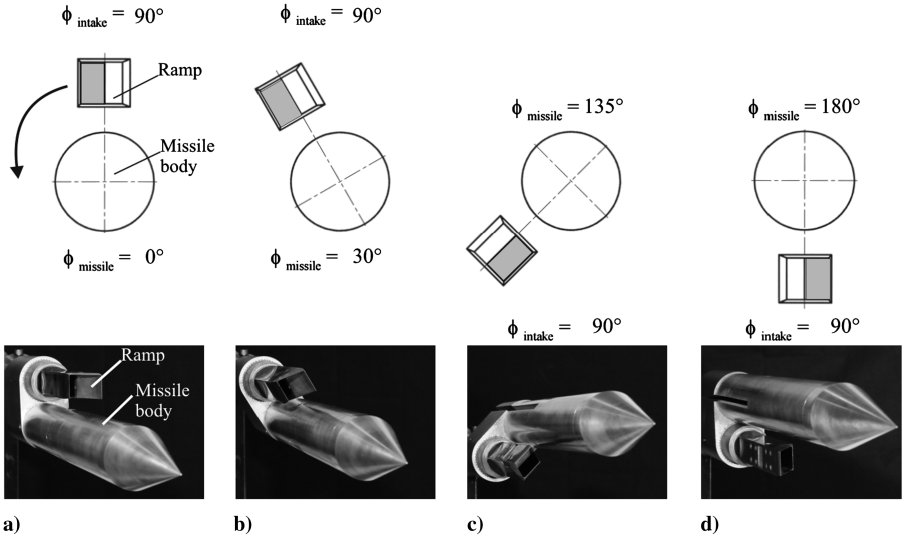

Fig. 3 Sketch of front view and photo of model at an roll angle of the intake of $\phi_{\text{intake}} = 90°$ and roll angles of the missile of a) $\phi_{\text{missile}} = 0°$, b) $\phi_{\text{missile}} = 135°$, c) $\phi_{\text{missile}} = 135°$, and d) $\phi_{\text{missile}} = 180°$.

moving the throttle, i.e., changing the critical throttle cross section (position 4 in Fig. 4). The throttle is controlled by a hydraulic system. Upstream of the throttle, the measurement pipe is fitted with pressure taps positioned at its end to measure the static pressure p_{st3} (position 3 in Fig. 4). This pressure value combined with the total temperature data and the critical throttle cross-section geometry are used for the calculation of the intake performance data. The exact position of the throttle is therefore determined with an integrated potentiometer whose output signal defines the variable throttle cross-sectional area A_4 (position 4 in Fig. 4). For further calculations, the continuity equation $\dot{m}_3 = \dot{m}_4$ is used with the following boundary conditions: The Mach number at the throttle cross-section 4 is $M_4 = 1$, isentropic flow of $T_{t3} = T_{t4}$ is assumed and the pressure loss is negligible, i.e., $p_{t3} = p_{t4}$. This yields

$$\frac{A_3}{A_4} = \frac{1}{M_3} \cdot \left(\frac{1 + \frac{\kappa-1}{2} \cdot M_3^2}{\frac{\kappa+1}{2}} \right)^{\frac{\kappa+1}{2(\kappa-1)}} \tag{3}$$

Using Eq. (3), M_3, which is needed for the mass flow ratio, can be calculated iteratively. The captured mass flow ratio is given by Eq. (4) multiplied by the calibration factor of 1 (idealized)

Table 1 Test conditions

α range, °	ϕ_{missile} range, °	ϕ_{intake} range, °	Missile length, L/D
0 . . . 30	0 . . . 180	0	5, 7, 9
0 . . . 30	0 . . . 180	90	5, 7, 9
0 . . . 30	0 . . . 180	180	5, 7, 9
0 . . . 30	0 . . . 180	270	5, 7, 9

Table 2 Freestream condition of mainstream condition

M_0	T_{t0}, K	p_{t0}, $\cdot 10^5$ Pa	Re, $\cdot 10^6$ m^{-1}
2.5	290	3.7	1.5

Table 3 Measurement inaccuracies

$\Delta M_0/M_0$, %	$\Delta T_{t0}/T_{t0}$, %	$\Delta p_{t0}/p_{t0}$, %	$\Delta Re/Re$, %
0.50	0.75	0.02	0.04

$$\frac{\dot{m}_3}{\dot{m}_0} = \frac{1}{\dot{m}_0} \cdot \frac{p_{t3}}{\sqrt{R \cdot T_{t0}}} \cdot A_3 \cdot M_3 \cdot \sqrt{\kappa} \cdot \left(1 + \frac{\kappa - 1}{2} \cdot M_3^2 \right)^{-\left(\frac{\kappa+1}{2(\kappa-1)}\right)} \tag{4}$$

where p_{t3} is

$$p_{t3} = p_{\text{st3}} \cdot \left(1 + \frac{\kappa - 1}{2} \cdot M_3^2 \right)^{\frac{\kappa}{\kappa-1}} \tag{5}$$

and $\dot{m}_3 = \rho_3 \cdot v_3 \cdot A_3$. The undisturbed mass flow $\dot{m}_0$ at $\alpha = 0°$ is calculated with the static pressure p_{st0} and static temperature p_{st0} with the projected intake plane A_0 perpendicular to the incident flow at M_0

$$\dot{m}_0 = \frac{p_{\text{st0}}}{\sqrt{R \cdot T_{\text{st0}}}} \cdot A_0 \cdot M_0 \cdot \sqrt{\kappa} \tag{6}$$

Pressure recovery is expressed as

$$\frac{p_{t3}}{p_{t0}} = \frac{p_{\text{st3}}}{p_{t0}} \cdot \left(1 + \frac{\kappa - 1}{2} \cdot M_3^2 \right)^{\frac{\kappa}{\kappa-1}} \tag{7}$$

The major measurement inaccuracies of the performance data mentioned above are presented in Table 4.

Both ratios (mass flow ratio and pressure recovery) are plotted on the intake characteristic diagram, as in Fig. 5:

The intake characteristic diagram shows the test procedure. At the beginning, the maximal mass flow ratio with low pressure recovery is detected while the throttle is open. During the test, the throttle closes continuously (arrow direction in Fig. 5). This event appears as a vertical increase with a nearly constant mass flow rate and rising pressure recovery (supercritical condition). The pressure rises as the throttle closes, during which the normal shock in the diffuser moves upstream. When the normal shock reaches the intake throat, the maximal pressure recovery (critical condition) is achieved. The theoretical maximal pressure recovery for a three-shock system with two oblique shocks and a normal shock at $M_0 = 2.5$ is 91% [16–18], where all oblique shocks are of equal strength [17]. With an increase in pressure, the shock leaves the intake and takes the form of a detached shock (subcritical condition) upstream. This shock in front of the intake entrance causes mass flow losses, since only part of the incident flow enters the intake and the other part is spillage. This detached shock can be stable at first. With further throttling, the shock becomes unstable until it finally jumps in and out of the intake. This unstable condition with pressure fluctuations is known as buzzing [19]. The buzzing is displayed (in Fig. 5) as a long, sloping zigzag pattern in the subcritical region. It is detected with a so-called RMS meter, whereas the buzzing value is normalized with p_{t0}. If this

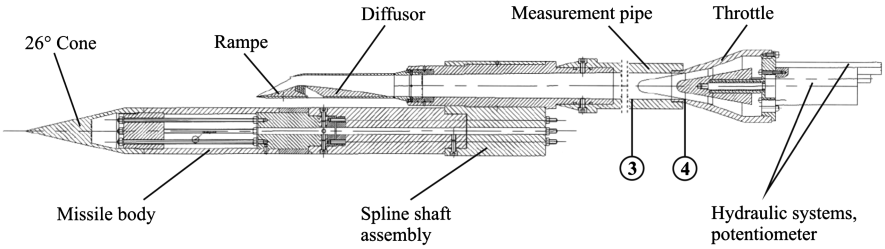

Fig. 4 Measurement configuration.

value becomes too large, the abort criterion is reached and the throttle opens at once. This response is necessary, since the pressure fluctuations can cause strong structural loads and can damage the model.

To investigate the flow effects, schlieren images [20] and oil flow visualization are used. Furthermore, the static pressure is measured on the main missile body. An additional cylindrical element equipped with 145 pressure taps was built for this purpose. The pressure taps are arranged in 13 rows, aligned in the x-axis direction with 10 mm gaps on the leeward and 20 mm gaps on the windward side. These rows are rotated in 15° steps ($\phi = 0°$ is the center of the leeward side). Inside the cylindrical element are thin tubes (Fig. 6, left) leading from the pressure taps to an electronic pressure-scanner.

To analyze the flow around the missile body and the inflow of the intake, the Pitot pressure is recorded with 7 Pitot rakes each with 12 Pitot tubes (Fig. 6, right). The quality of Pitot pressure measurement is affected by the angle between the tube and the flow direction. The results below 10° are not significantly affected by the measurement error [21]. To compensate these errors, the Pitot rake was measured alone (without the missile body) over all angles of attack.

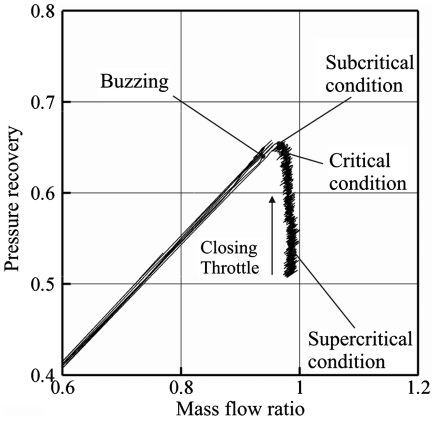

Fig. 5 Example of the intake characteristic diagram.

III. Experimental Results

A. Effects of Missile Length

Tests were first conducted while varying the axial position of the intake along the missile, where, for example, boundary separation and leeward flow effects as well as windward flow effects are analyzed. The results of the leeward flow is demonstrated in Fig. 7 (left). The intake is positioned (as an example) at the leeward center with an intake roll angle of $\phi_{\text{intake}} = 90°$ (in relation to the missile's surface). The intake's characteristics display a distinct loss in mass flow and pressure recovery when the intake position is moved downstream.

The differences in pressure recovery and mass flow rate between the $L/D = 5$ (Fig. 7a, left) and $L/D = 9$ (Fig. 7c, left) configurations are about 24% and about 38%, respectively. At an angle of attack of $\alpha = 30°$ Fig. 7 (right), the differences are 0.8% for pressure recovery and 2.3% for the mass flow rate. But compared with the reference condition (at $\alpha = 0°$), the performance drop is significant (>80% for the mass flow rate). It is caused by strong flow separation at the leeward side at such high angles of attack.

Figure 8 shows the influence of different angles of attack on the mass flow ratio in a supercritical operation regime (which is mainly referred to in the following) over angles of attack between $0° \leq \alpha \leq 30°$ for the three axial positions.

On the leeward side at small angles of attack up to 9°, the mass flow ratio (Fig. 8a, left) and pressure recovery (Fig. 8b, left) are almost the same for all three configurations, since the change in the flow direction is negligible with respect to the intake ramps. This implies constant intake compression and accordingly a constant mass flow rate. At larger angles of attack, the mass flow rate (and pressure recovery) at the upstream position of $L/D = 5$ drops at higher angles. The drops in mass flow ratio (and pressure recovery) at e.g., $\alpha = 15°$ are larger when the intake positions are further downstream. On the windward side in Fig. 8 at small angles of attack, the mass flow ratio (Fig. 8a, right) and pressure recovery (Fig. 8b, right) are almost equal to the leeward side. At higher angles of attack the inclined position of the intake's side walls (ramp-like) seems to increase the mass flow and pressure recovery. The intake positions $L/D = 7$ and $L/D = 9$ (on the windward side) are nearly congruent. Comparing the upstream position of $L/D = 5$ with the other two downstream positions, a variation of less than 3% is detected. A possible explanation is the upstream influence of the cone flow.

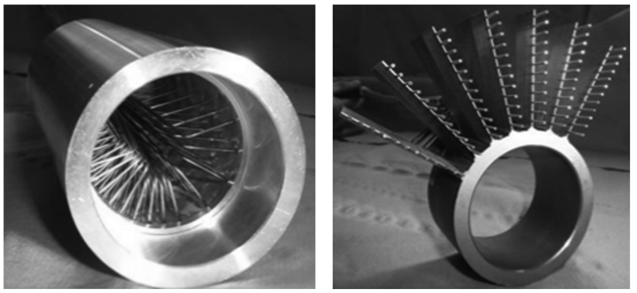

Fig. 6 Inside view of the cylindrical element (left) and Pitot rakes (right).

To understand the leeward drop in mass flow at higher angles of attack, Fig. 9 shows the comparison between $\alpha = 15$ and 18° for $L/D = 5$. In Fig. 9a (the $\alpha = 15°$ case), a boundary-layer separation is visible in the upper schlieren image. It is situated between the intake and missile body and does not enter the intake. This is also confirmed by the Pitot pressure measurement shown below.

Table 4 Measurement inaccuracies of throttle device

$\Delta p_{st3}/p_{st3}$, %	$\Delta A_3/A_3$, %	$\Delta(p_{t3}/p_{t0})/(p_{t3}/p_{t0})$, %	$\Delta(\dot{m}_3/\dot{m}_0)/(\dot{m}_3/\dot{m}_0)$, %
0.02	0.03	0.03	1.69

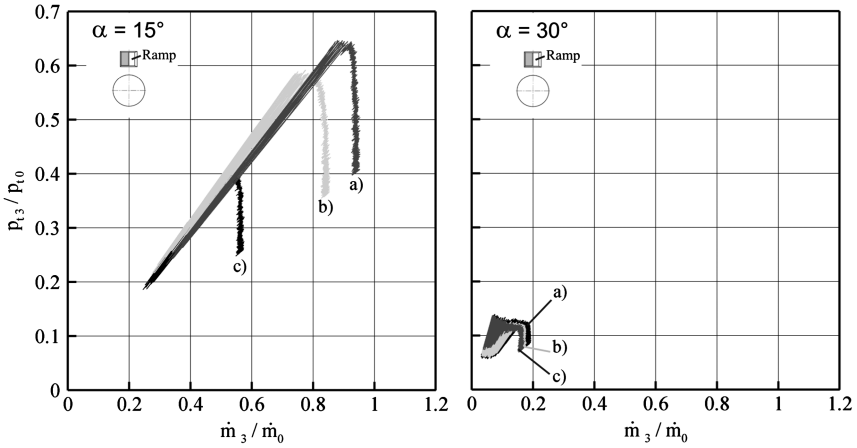

Fig. 7 Characteristic intake performance of $\phi_{\text{intake}} = 90°$, $\phi_{\text{missile}} = 0°$, and $\alpha = 15°$ (left), $\alpha = 30°$ (right) at $M_0 = 2.5$ and a) $L/D = 5$, b) $L/D = 7$, c) $L/D = 9$.

It displays regions of low pressures that do not enter the intake. Figure 9b, on the other hand, shows the influence of flow separation (see schlieren images) and the regions of low pressure (Pitot measurements), which are interpreted as leeward vortices. These enter the intake and cause mass flow losses of about 11% (see Fig. 8) and pressure recovery losses of about 4%.

Representative of the differences in flow development around the missile body are the results of the Pitot measurements at an angle of attack of $\alpha = 15°$. Comparing the three missile positions (at $L/D = 5, 7, 9$) at 15°, the differences in mass flow loss are clearly visible in Fig. 8. The intake position $L/D = 5$, as explained above, is barely affected by the pressure losses (see blue values in Fig. 9a). However, it is easy to imagine the influence of the vortices growing when the intake is moved downstream. Figure 10a shows the results of the Pitot measurements of $L/D = 7$, which indicate the consequence of developing vortices. This vortices disturb the intake flow and therefore cause a mass flow loss. These disturbances are displayed (in Fig. 10) as regions of low pressure. At $L/D = 9$ (Fig. 10b), the vortices enclose the intake and the pressure losses extend over the intake area, causing an increasing mass flow loss.

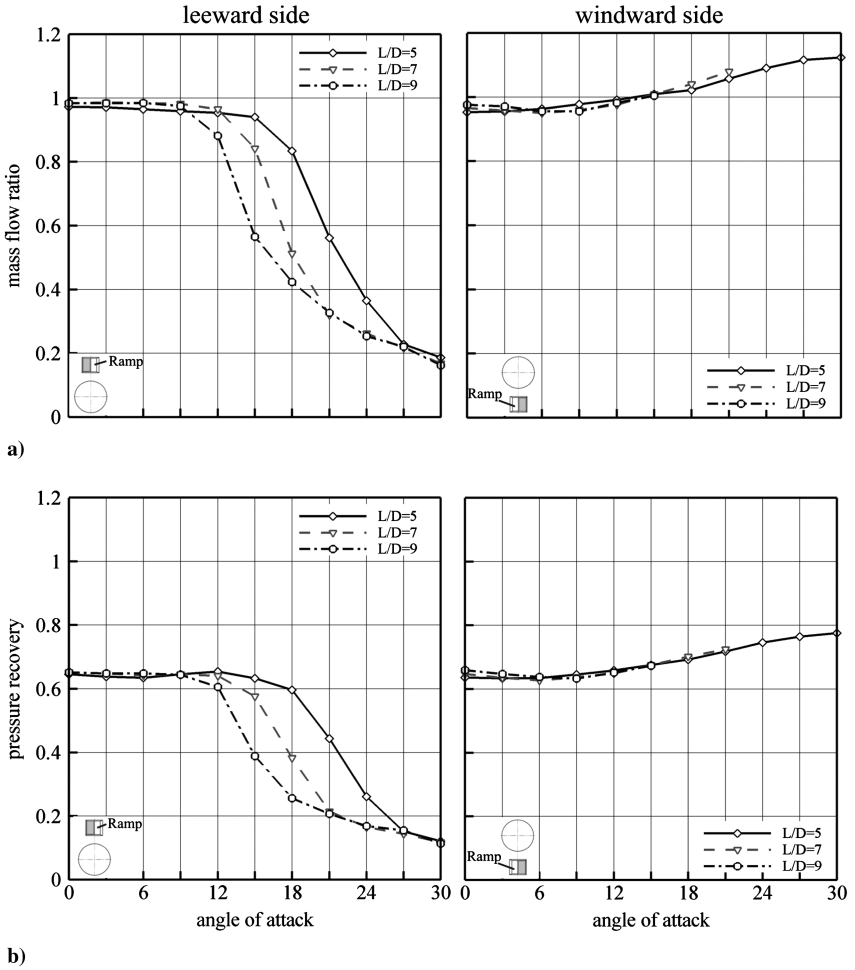

Fig. 8 Variation of axial position in relation to a) the mass flow ratio, and b) pressure recovery relating to the leeward side at $\phi_{\text{missile}} = 0°$ (left) and windward side at $\phi_{\text{missile}} = 180°$ (right), $\phi_{\text{intake}} = 90°$ and $M_0 = 2.5$.

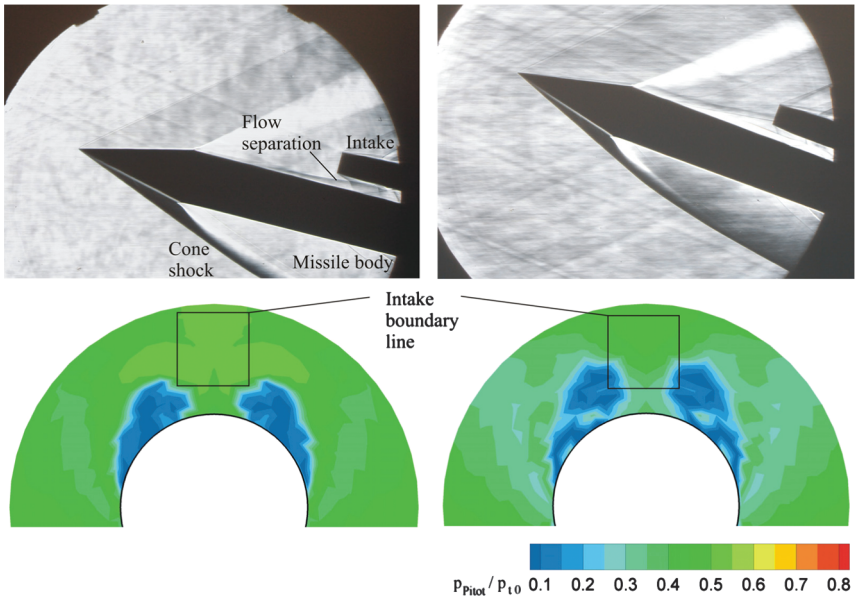

a) $\alpha = 15°$ b) $\alpha = 18°$

Fig. 9 Schlieren image and Pitot pressure profile (mirrored) at a) $\alpha = 15°$, and b) $\alpha = 18°$, $L/D = 5$, $M_0 = 2.5$.

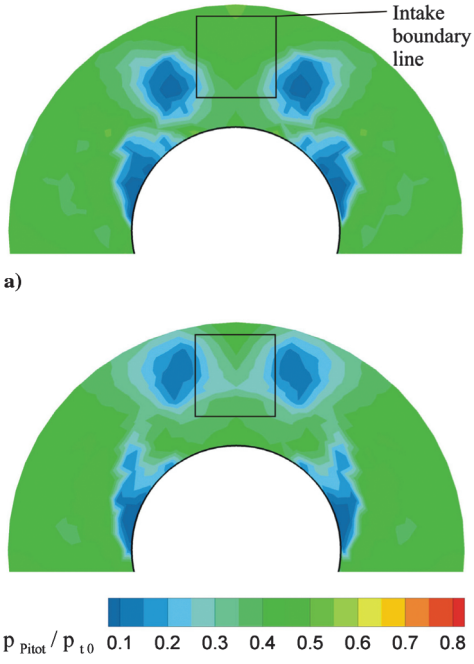

Fig. 10 Pitot pressure profiles (mirrored) at $M_0 = 2.5$ and $\alpha = 15°$: a) $L/D = 7$, and b) $L/D = 9$.

To gain a better impression of flow development over the whole missile body, the flow field is visualized with the oil flow method. Figure 11 shows the streamlines caused on the surface on the leeward side. The surface streamlines are symmetrical and their pattern reveals counter-rotating vortices (taking account of [22]) that cause mass flow and pressure losses. These vortices also develop from the apex of the cone [5,22,23], which means that the position of the intake is of great importance. Downstream, the oil flow image is more complex and indicates primary and secondary vortices. Regarding the leeward surface streamlines, a conspicuous feature is the sharp black lines on the surface where the paint has been wiped off. The black lines seem to be an indication of embedded shocks [24] or of vortex-induced shocks. These kinds of shocks are also found in a similar investigation, see [25].

Figure 11 shows corresponding static pressure coefficients, which are calculated using measured pressure with a Pressure Systems, Inc., system and apply the following relationship [26]

$$c_P = \frac{p_{\mathrm{st}} - p_{\mathrm{st0}}}{\frac{\kappa}{2} \cdot p_{\mathrm{st0}} \cdot M_0^2} \tag{8}$$

where the static pressure of the incident flow is calculated with

$$p_{\mathrm{st0}} = p_{t0} \cdot \left(1 + \frac{\kappa - 1}{2} M_0^2\right)^{-\frac{\kappa}{\kappa - 1}} \tag{9}$$

The negative pressure coefficient values on the leeward center are caused by the separated flow and vortices [22].

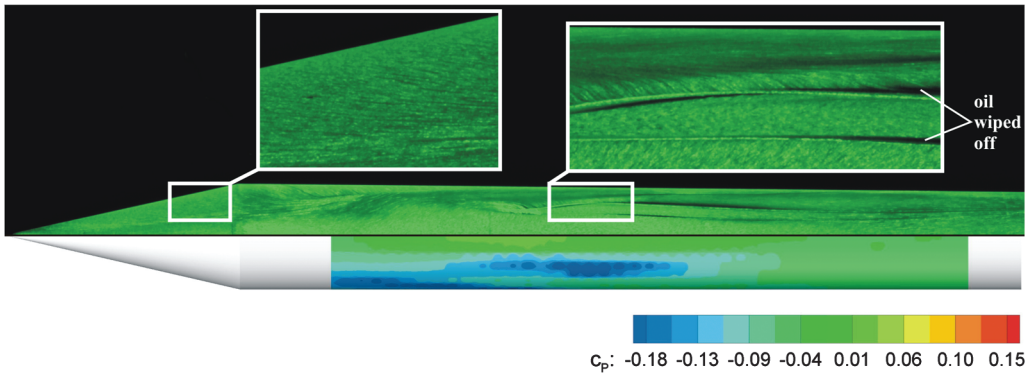

Fig. 11 Top view of leeward side: oil flow image (top) and distribution of pressure coefficient (bottom) at $M_0 = 2.5$ and $\alpha = 15°$.

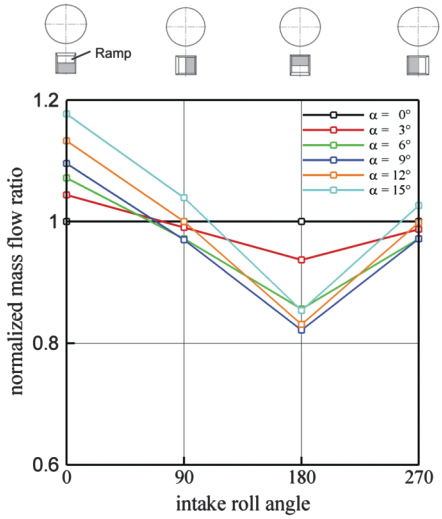

Fig. 12 Normalized mass flow ratio diagram of $\phi_{\text{missile}} = 180°$, $L/D = 9$, $M_0 = 2.5$.

The leeward flow strongly affects intake performance. For the leeward side at least, the effect of the variation in the axial intake position must not be underestimated. Considering a given missile length, intake performance is better if it is positioned in the upstream part. Unfortunately, this also necessitates a long channel (diffuser) connecting the intake to the combustion chamber. It has also a negative impact on the internal aerodynamics, e.g., higher friction, stronger flow separation and pressure losses. In addition the missile's weight will also grow.

B. Effects of Intake Roll

Because of the flow separation problems described above, the intakes are mainly mounted on the windward surface of the missile. This chapter of the paper is therefore devoted to the windward side flow phenomena. The intake's external compression depends on the angle between the flow and the intake ramps. To focus on the intake's compression, the following analyses relate to the intake located on the windward side. For the first tests, the intake was therefore placed at $\phi_{\text{missile}} = 180°$ position. Figure 12 shows the effect of varying intake roll angle at angles of attack between 0 and 15°. To compare the supercritical mass flow ratios for the intake's roll angles of $\phi_{\text{intake}} = 0$, 90, 180, and 270°, the mass flow ratio is normalized with the mass flow ratio of the respective roll angle at the design angle of attack of $\alpha = 0°$. Thus, the normalized mass flow ratio is expressed as

$$\frac{\text{mass flow ratio of } \alpha}{\text{mass flow ratio of } \alpha = 0°} = \frac{\frac{\dot{m}_3}{\dot{m}_0}}{\frac{\dot{m}_{3,\alpha=0°}}{\dot{m}_0}} = \frac{\dot{m}_3}{\dot{m}_{3,\alpha=0°}} \tag{10}$$

The intake with the roll angles of $\phi_{\text{intake}} = 90$ and 270° is symmetrical and therefore the mass flow rates are almost identical.

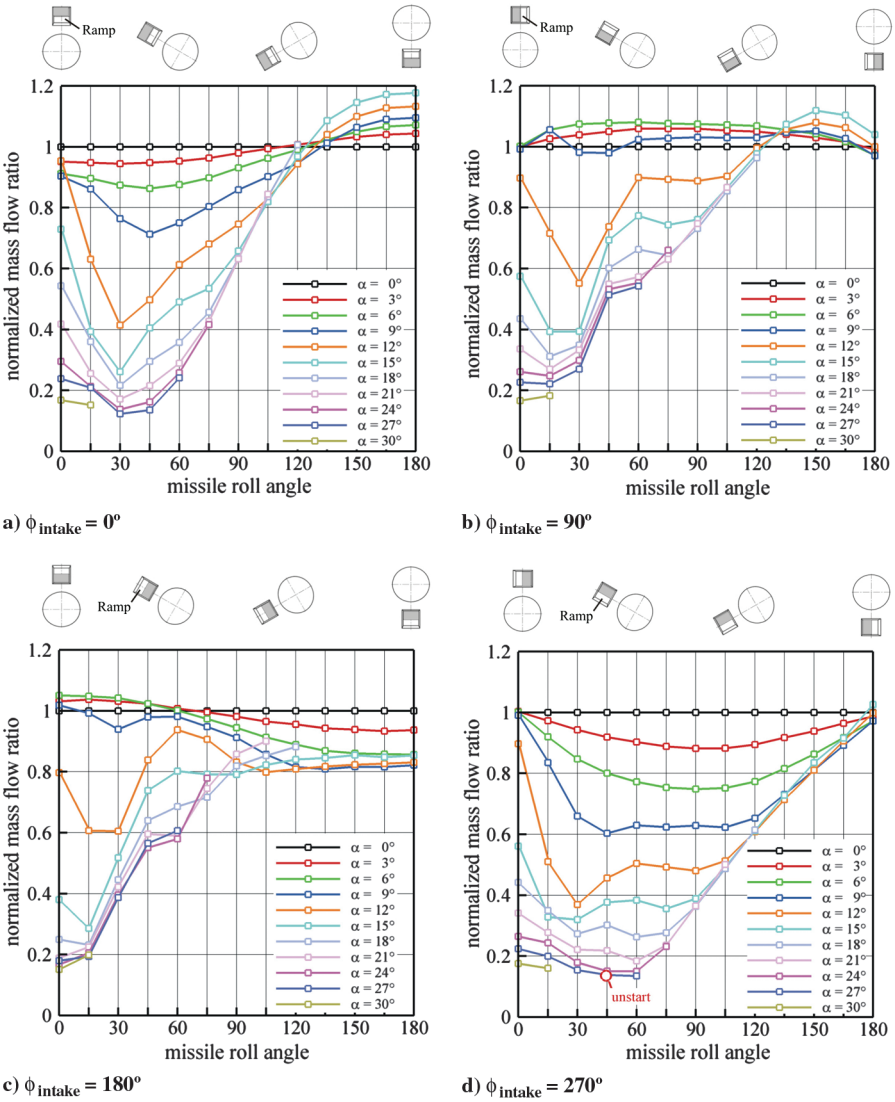

a) $\phi_{\text{intake}} = 0°$ b) $\phi_{\text{intake}} = 90°$

c) $\phi_{\text{intake}} = 180°$ d) $\phi_{\text{intake}} = 270°$

Fig. 13 Normalized mass flow ratio diagram of a) $\phi_{\text{intake}} = 0°$, b) $\phi_{\text{intake}} = 90°$, c) $\phi_{\text{intake}} = 180°$, and d) $\phi_{\text{intake}} = 270°$, $L/D = 9$, $M_0 = 2.5$.

But the characteristics at intake roll angles of $\phi_{\text{intake}} = 0°$ and 180° are entirely different. At $\phi_{\text{intake}} = 0°$, the angle between flow direction and ramp angle rises in contrast to the $\phi_{\text{intake}} = 180°$ configuration, where this angle is reduced, i.e., the compression of the $\phi_{\text{intake}} = 0°$ configuration increases and consequently the mass flow rate as well.

Because there is an obvious dependency of intake performance on the intake roll angle, further detailed analyses were performed at different roll angles and are described below.

C. Effects of the Main Missile Body Roll Angle

First the intake is rolled around the missile body with a fixed intake roll angle at $L/D = 9$. For better comparison, the mass flow ratio is normalized with the value at $\alpha = 0°$ [see Eq. (10)]. The results for all four intake roll angles are shown in Fig. 13.

Large mass flow losses are apparent at missile body roll angles of $\phi_{\text{missile}} < 90°$. As described in Sec. III.A, these losses are mainly caused by the leeward vortices. The diagrams with the intake roll angles of $\phi_{\text{intake}} = 90°$ (Fig. 13b) and 180° (Fig. 13c) show an increase at the normalized mass flow ratio (i.e., smaller losses) with increasing missile body roll angle ϕ_{missile}. The reason for this is the growing ramp angle with respect to the approaching flow with growing angle of attack α. Hence, an increase in compression causes a growing mass flow.

A reduction in the mass flow rate caused by a decrease in compression was measured at the intake roll angle of $\phi_{\text{intake}} = 270°$ (see Fig. 13d). This configuration is an exception, because its reference at $\alpha = 0°$ shows better performance for the full range of missile roll angles $0° < \phi_{\text{missile}} < 180°$. In contrast, the configuration $\phi_{\text{intake}} = 90°$ features better compression and therefore better performance. On account of the growing angle of attack, the angle between incident flow and intake ramp grows with the $\phi_{\text{intake}} = 90°$ and falls with the $\phi_{\text{intake}} = 270°$ configuration. Note that in Fig. 13d at $\alpha = 27°$ and $\phi_{\text{missile}} = 45°$, the intake does not start, i.e., even with an open throttle (Sec. II.C) the back pressure can be too large.

On the windward side mass flow losses are also present, e.g., the $\phi_{\text{intake}} = 180°$ configuration at a missile roll angle of $\phi_{\text{missile}} = 180°$ in Fig. 13c. This reduction in the mass flow rate is not only caused by reducing the ramp angle with respect to the approaching flow with growing angle of attack α, but also caused by the decrease of the projected cross section created by the leading edge of the ramp and the edge of the cowl, where the upstream leading edge of the ramp is blocking the incident flow. Rolling the intake to a intake roll angle of $\phi_{\text{intake}} = 0°$ at a missile roll angle of $\phi_{\text{missile}} = 180°$, the upstream leading edge of the ramp is not blocking the incident flow anymore. With growing angle of attack α the projected cross section (between the leading edge of the ramp and the edge of the cowl) is increasing and causes a growing mass flow, which is shown in Fig. 13a.

Looking at all four diagrams at Fig. 13, the difference between $\alpha = 9°$ and 12° is conspicuous and clearly visible at a missile body roll angle of, for example, $\phi_{\text{missile}} = 30°$. To analyze this effect, schlieren images and Pitot measurements were carried out at these angles of attack. At $\alpha = 9°$ a flow separation is visible in the schlieren image (see Fig. 14). The Pitot rake is located at the intake position. The Pitot pressure data show a region of low pressure which interacts with the intake boundary line. Figure 15 shows a more enhanced flow separation at an angle of attack of 12°. The vortex-embedded flow completely enters the intake and, as shown in the Pitot diagram, changes the pressure distribution inside the intake considerably.

At missile body roll angles of $\phi_{\text{missile}} > 90°$, the incident flow is influenced, amongst other things, by the cone shock. The resulting intake performance depends on its compression, which increases for intakes with a roll angle of $\phi_{\text{intake}} = 0°$ (Fig. 13a) and 90° (Fig. 13b). Noticeable is the rise in mass flow above the reference line ($\alpha = 0°$) at small angles of attack. At a missile roll angle of $\phi_{\text{missile}} = 135°$, the mass flow ratio is greater than 1 at.all angles of attack. To ensure good performance over the whole angle-of-attack range, the intake should be positioned at missile roll angles of $135° \leq \phi_{\text{missile}} \leq 180°$, i.e., on the windward side.

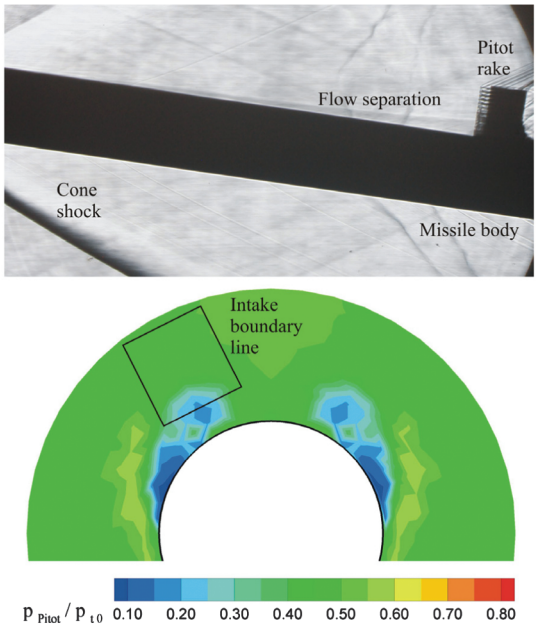

Fig. 14 Schlieren image and Pitot pressure profile (mirrored) of $\phi_{\text{missile}} = 30°$ at $\alpha = 9°$, $L/D = 9$, $M_0 = 2.5$.

D. Missile Configurations

Based on the results of the tests described above, two missile configurations have been identified as more feasible. The chosen configurations have intake roll angles of $\phi_{\text{intake}} = 0°$ and 90°, which have better characteristics than the other two with intake roll angles of $\phi_{\text{intake}} = 180°$ and 270°. The intake is located at the rear axis position ($L/D = 9$) at an missile roll angle of $\phi_{\text{missile}} = 135°$. At this downstream intake position, its distance from the combustion chamber is short and the interference of a symmetrical two-intake configuration is negligible. Furthermore, the intake performance between the three axial positions are similar on the windward side (results of Sec. III.A).

Figure 16 shows the supercritical mass flow ratio calculated with Eq. (10) for the configurations $\phi_{\text{intake}} = 0°$ and $\phi_{\text{intake}} = 90°$ over a large angle-of-attack range of $-27° \leq \alpha \leq 15°$ (results of Sec. II.C).

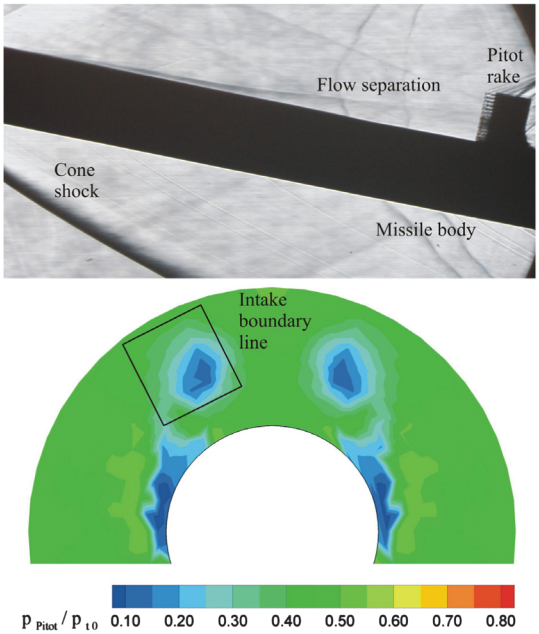

Fig. 15 Schlieren image and Pitot pressure profile (mirrored) of $\phi_{\text{missile}} = 30°$ at $\alpha = 12°$, $L/D = 9$, $M_0 = 2.5$.

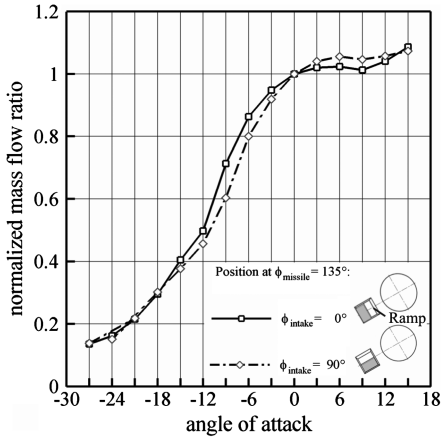

Fig. 16 Normalized mass flow ratio of $\phi_{intake} = 0°$ and 90° at $\phi_{missile} = 135°$, $L/D = 9$, $M_0 = 2.5$.

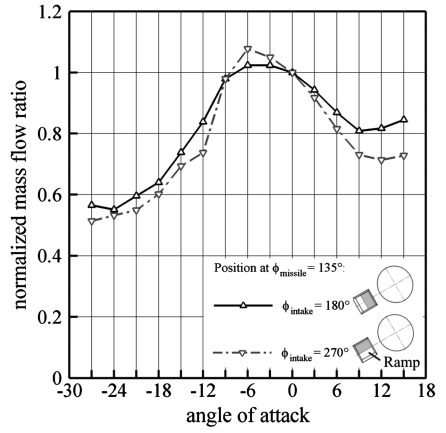

Fig. 17 Normalized mass flow ratio of $\phi_{intake} = 180°$ and 270° at $\phi_{missile} = 135°$, $L/D = 9$, $M_0 = 2.5$.

For negative angles of attack the symmetry of the configurations is used.

At positive angles of attack the intake's compression yields an increase in mass flow ratio. The $\phi_{intake} = 90°$ configuration has a mass flow ratio up to 3.4% higher than the $\phi_{intake} = 0°$ configuration. On the leeward side with rising negative angles of attack, the intake's compression decreases, the side wall and the leading edge of the ramp is partially blocking the incident flow and consequently the mass flow rate decreases. Here the $\phi_{intake} = 0°$ configuration has a higher mass flow ratio with a maximum difference of 11%. These two configurations can be used if high intake performance during maneuvers at positive angles of attack is required. (Note that these differences are due in small part to intake position and in large part to intake design itself.)

Nevertheless, if the main objective is good performance in maneuvering flight at negative angles of attack, the intake roll angles are preferably $\phi_{intake} = 180°$ and 270°, as can be seen in Fig. 17.

At negative angles of attack, the intake compression increases at small angles at which the vortices are not strongly developed. But as mentioned in the previous section, this angle-of-attack region is small compared with the higher negative angles of attack, where the mass flow decreases significantly. Thus, the maneuvering capability of agile missiles would be limited except within this small angle-of-attack region.

(Note: There are other configuration which could be considered, e.g., the $\phi_{intake} = 45°$ configuration at $\phi_{missile} = 135°$. Its performance should be better for positive angles of attack. Though, for a actual application additional structures need to be placed between intake and missile. Attaching the intake tube to the missile, the missile's front surface increases which results in a larger drag compared with the present configurations.)

IV. Conclusions

The intake's performance at different positions around the missile body has been studied in the TMK. Systematic experiments were carried out by varying the axial position of the intake, the intake roll angle and the missile roll angle. All tests were performed at the intake design Mach number of 2.5 within an angle-of-attack range of $-30° \leq \alpha \leq 30°$. Besides the measurement of the main intake performance parameters, i.e., mass flow rate and pressure recovery, static and Pitot pressure were measured and the flow was visualized using schlieren and oil flow techniques.

The intake shows differences in performance at different angles of attack ($-30° \leq \alpha \leq 30°$) when its axial position is varied along the missile body. Furthermore, intake performance shows a strong dependency on intake roll angle ($0° \leq \phi_{intake} \leq 270°$) and missile roll angle ($0° \leq \phi_{missile} \leq 180°$). The main reasons for these differences are the complex flow phenomena around the missile, e.g., flow separation, vortex formation, etc., and varying projected intake cross section and intake compression.

Two main flow phenomena affecting intake performance have been identified. On the leeward side the intake performance is poor even at intake roll angles of $\phi_{intake} = 90°$ and 180° with a higher external compression. The vortices develop from the apex of the missile cone and expand over the missile length, resulting in losses of mass flow and pressure recovery. On the contrary, the dominant effect on the windward side is the higher external compression of the intake with $\phi_{intake} = 0°$ and 90°. This compression leads to an increase in mass flow and pressure recovery at a missile body roll angle of about $\phi_{missile} = 135°$ for almost every angle of attack.

The preferred position is on the windward side, where better performance (at positive α) than for the design condition at $\alpha = 0°$ is achieved. It is possible to mount two intakes on the windward side of the missile symmetrically and 90° apart from each other seem to yield the ideal performance for a ramjet. A downstream intake position close to the combustion chamber is more favorable because of better internal aerodynamics and less weight.

Acknowledgments

This study was carried out in the context of the DLR project Advanced Missile Technology (FFT: Fortschrittliche Flugkörper-Technologien). The authors gratefully acknowledge the support of the German Ministry of Defense and the DLR Aeronautics and Energy Program Directorate.

References

[1] Seddon, J., and Goldsmith, E. L., *Intake Aerodynamics*, AIAA Education Series, AIAA, New York, 1985, Chap. 13.

[2] Seddon, J., and Goldsmith, E. L., *Practical Intake Aerodynamic Design*, AIAA Education Series, AIAA, New York, 1993, Chaps. 5, 8.

[3] Neal, M. C., and Lamb, P. S., "Some Test with Variable Ramp Intake Having Sidewall Compression and Design Mach Number of 2.2," Aeronautical Research Council, ARC/CP-936, London, 1967.

[4] Neal, M. C., and Lamb, P. S., "Some Test with Variable Ramp Intake Having Combined External/Internal Compression, and a Design Mach Number of 2.2," Aeronautical Research Council, ARC/CP-805, London, 1962.

[5] Herrmann, D., Triesch, K., and Gülhan, A., "Experimental Study of Chin Intakes for Airbreathing Missiles with High Agility," *Journal of Propulsion and Power*, Vol. 24, No. 2, March–April 2008, pp. 236–244. doi:10.2514/1.29672

[6] Hirschen, C., Herrmann, D., and Gülhan, A., "Experimental Investigation of the Performance and Unsteady Behavior of a Supersonic Intake," *Journal of Propulsion and Power*, Vol. 23, No. 3, May–June 2007, pp. 566–574. doi:10.2514/1.25103

[7] Colville, J. R., Starkey, R. P., and Lewis, M. J., "Extending the Flight Number of the SR-71 Inlet," AIAA Paper 2005-3284, 2005.

[8] Kojima, T., Sato, T., Sawai, S., and Tanatsugu, N., "Experimental Study on Restart Control of A Supersonic Air-Breathing Engine," *Journal of*

Propulsion and Power, Vol. 20, No. 2, March–April 2004, pp. 273–279. doi:10.2514/1.9253

[9] Kojima, T., Tanatsugu, N., Sato, T., and Enomoto, Y., "Experimental Study on Inlet Control System for Hypersonic Flight," *Japan Society of Aeronautical and Space Science and ISTS*, International Symposium on Space Technology and Science Paper 200-a-08, 2000, pp. 48–53.

[10] Kojima, T., Sato, T., Sawai, S., and Tanatsugu, N., "Experimental Study on Restart Control of a Supersonic Air-Breathing Engine," *Journal of Propulsion and Power*, Vol. 20, No. 2, March–April 2004, pp. 273–279. doi:10.2514/1.9253

[11] Esch, H., "The $0,6\ \text{m} \times 0,6\ \text{m}$ Trisonische Meßstrecke (TMK) of the DFVLR in Köln-Porz (Status 1986)," ESA TT-1052, June 1987;also "Die $0,6\ \text{m} \times 0,6\ \text{m}$: Trisonische Meßstrecke (TMK) der DFVLR in Köln-Porz (Stand 1986)," DFVLR-Mitt, 86-21, Köln, 1986.

[12] Van Wie, D. M., "Scramjet Inlets," *Scramjet Propulsion*, edited by E. T. Curran, S. N. B. Murthy, AIAA Progress in Astronautics and Aeronautics, AIAA, Reston, VA, 2000, pp. 447–511.

[13] Kantrowitz, A., and Donaldson, C. duP., "Preliminary Investigation of Supersonic Diffusers," NACA Wartime Rept. No. WR L-713, Washington, D. C., 1945.

[14] Anon., "Durchflussmessung von Fluiden mit Drosselgeräten in voll durchströmten Leitungen mit Kreisquerschnitt: Teil 1: Allgemeine Grundlagen und Anforderungen," Deutsche Fassung EN ISO 5167-1:2003, Deutsches Institut für Normung, e. V., Beuth Verlag GmbH, Berlin, Jan. 2004; also "Measurement of Fluid Flow by Means of Pressure Differential Devices Inserted in Circular Cross-Section Conduits Running Full: Part I: General Principles and Requirements," ISO 5167-12003 (in English).

[15] Anon., "Durchflussmessung von Fluiden mit Drosselgeräten in voll durchströmten Leitungen mit Kreisquerschnitt—Teil 2: Blenden," Deutsche Fassung EN ISO 5167-2:2003, DIN Deutsches Institut für Normung, e. V., Beuth Verlag GmbH, Berlin, Jan. 2004; also "Measurement of Fluid Flow by Means of Pressure Differential Devices Inserted in Circular Cross-Section Conduits Running Full: Part II: Orifice Plates," ISO51672:2003 (in English).

[16] Hünecke, K., "Flugtriebwerke: Ihre Technik und Funktion," 1. Auflage, Motorbuch Verlag, Stuttgart, 1976.

[17] Oswatitsch, K., "Der Druckrückgewinn bei Geschossen mit Rückstoßantrieb bei hohen Überschallgeschwindigkeiten (Der Wirkungsgrad von Stoßdiffusoren)," Forschungen und Entwicklungen des Heereswaffenamtes, Rept. 1005, Göttingen, Germany, 1944; reprint: Deutsche Versuchsanstalt für Luftfahrt, e. V., Bericht Nr. 49, Dec. 1957; also: "Pressure Recovery for Missiles with Reaction Propulsion at High Supersonic Speed (The Efficiency of Shock Diffusers)," NACA TM-1140, June 1947 (in English).

[18] Goldsmith, E. L., and Seddon, J., *Practical Intake Aerodynamic Design*, AIAA Education Series, AIAA, Washington D. C., 1993, pp. 1–20.

[19] Krohn, E.-O., "Inlet Buzz in Ramjets and its Suppression," *AIAA Eighth International Symposium on Air Breathing Engines (ISABE) in Cincinnati, OH, ISABE 87-7006*, AIAA, New York, 1987, pp. 110–117.

[20] Settles, G. S., *Schlieren and Shadowgraph Techniques: Visualizing Phenomena in Transparent Media*, Springer–Verlag, Berlin, 2001.

[21] Nitsche, W., *Strömungsmeßtechnik*, Springer–Verlag, Berlin, 1994.

[22] Peak, D. J., and Tobak, M., "Three-Dimensional Interactions and Vortical Flows with Emphasis on High Speeds," *North American Treaty Organization Advisory Group for Aerospace Research and Development*, AGARDograph No. 252, London, July 1980.

[23] Herrmann, D., and Triesch, K., "Experimental Investigation of Isolated Inlets for High Agile Missiles," *Aerospace Science and Technology*, Vol. 10, Issue 8, Dec. 2006, pp. 659–667. doi:10.1016/j.ast.2006.05.004

[24] Boersen, S. J., "Reynolds Number Effects on Pressure and Normal Force Distributions Along Conically Pointed Circular Cylinder at Freestream Mach Number of 2.3," National Aerospace Laboratory, NLR TR 75124 U, Netherlands, 1975.

[25] Seshadri, S. N., and Narayan, K. Y., "Possible Types of Flow on Lee-Surface of Delta Wings at Supersonic Speeds," *The Aeronautical Journal*, Vol. 92, No. 915, May 1988, pp. 185–199.

[26] Anderson, J. D. Jr., "Hypersonic and High-Temperature Gas Dynamics," 2nd ed., AIAA Education Series, AIAA, Reston, VA, 2006.

F. Liu
Associate Editor